Influence of subglacial drainage system evolution on glacier surface motion: Haut Glacier d'Arolla, Switzerland

Douglas Mair,[1,2] Peter Nienow,[3] Martin Sharp,[1] Trudy Wohlleben,[1] and Ian Willis[4]

Received 12 March 2001; revised 23 October 2001; accepted 28 October 2001; published XX Month 2002.

[1] The relationship between the evolution of subglacial drainage system morphology and spatial patterns of glacier surface velocity was investigated using dye tracing experiments and ground surveying throughout the 1995 melt season at Haut Glacier d'Arolla, Switzerland. With the onset of high and variable melt season discharges, subglacial drainage changed from a predominantly distributed system to a predominantly channelized system. The change occurred later farther up glacier. During the period of drainage evolution the glacier was subjected to three periods of rapidly rising meltwater discharge. The magnitude and spatial pattern of the glacier's velocity response differed between these periods and can be explained in terms of the impact of the evolving drainage system morphology on the amplitude and spatial distribution of basal hydrological forcing. Increasing discharge through a distributed drainage system caused widespread basal forcing and high glacier velocity. Increasing discharge through incipient channels below moulins, not yet connected to the main channel, caused more localized basal forcing and slightly increased glacier velocity. Increasing discharge through a fully channelized drainage system caused no significant basal forcing and glacier velocity was not significantly different from the annual deformation flow pattern. Empirical orthogonal function analysis of flow patterns defined two distinct spatial modes of surface velocity which corresponded closely with the drainage system morphologies inferred to be present during each event. The relative importance of these modes changed through the melt season, suggesting a temporal change in the spatial pattern of hydrologically induced basal forcing. *INDEX TERMS:* 1655 Global Change: Water cycles (1836); 1719 History of Geophysics: Hydrology; 1827 Hydrology: Glaciology (1863); 1863 Hydrology: Snow and ice (1827); *KEYWORDS:* glacier motion, subglacial hydrology, dye tracing

1. Introduction

[2] In this paper, we utilize the results of surface velocity surveys and dye tracing experiments to investigate the impact of seasonal changes in the morphology of a subglacial drainage system on the amplitude and spatial pattern of a glacier's velocity response to periods of increasing meltwater runoff. Variations in subglacial water pressure can cause variations in basal motion by sliding [*Iken*, 1981; *Iken and Bindschadler*, 1986; *Hooke et al*, 1989; *Hanson et al.*, 1998] or by bed deformation [*Boulton and Hindmarsh*, 1987; *Truffer et al.*, 2001]. The relationship between water pressure and discharge varies with the type of subglacial drainage system [*Röthlisberger*, 1972; *Walder*, 1986; *Kamb*, 1987]. Therefore the relationship between glacier motion and discharge will change if the drainage system changes. Theoretical and field-based studies of glacier hydrology suggest that a subglacial drainage system can evolve throughout a melt season from a hydraulically inefficient, distributed drainage system to a hydraulically efficient, channelized system [*Hock and Hooke*, 1993; *Nienow et al.*, 1998]. There is empirical evidence that the evolution is associated with the up-glacier retreat of the snow line which exposes new moulins and crevasses, subjecting them to high-magnitude and diurnally variable surface runoff from impermeable, low-albedo ice surfaces [*Nienow et al.*, 1998]. Dye tracing experiments [*Hock and Hooke*, 1993; *Nienow et al.*, 1998] and borehole water level measurements [*Fountain*, 1994; *Hubbard et al.*, 1995; *Gordon et al.*, 1998] suggest that channelized and distributed drainage systems can coexist. Seasonal changes in drainage system type will therefore change the spatial pattern of subglacial hydrological forcing. Many of the existing theories of subglacial water pressure and its effect on basal motion are concerned with processes occurring at scales of the order of a few meters reflecting the scale of basal cavities, channels, or bed form irregularities [*Lliboutry*, 1979; *Iken*, 1981; *Walder*, 1986; *Kamb*, 1987; *Humphrey*, 1987]. The basal motion response to hydrological forcing is often interpreted from changes in

[1]Department of Earth and Atmospheric Sciences, University of Alberta, Edmonton, Alberta, Canada.
[2]Now at Department of Geography and Environment, University of Aberdeen, Aberdeen, UK.
[3]Department of Geography and Topographic Sciences, University of Glasgow, Glasgow, UK.
[4]Department of Geography, University of Cambridge, Cambridge, UK.

0148-0227/02/2001JB000514$09.00

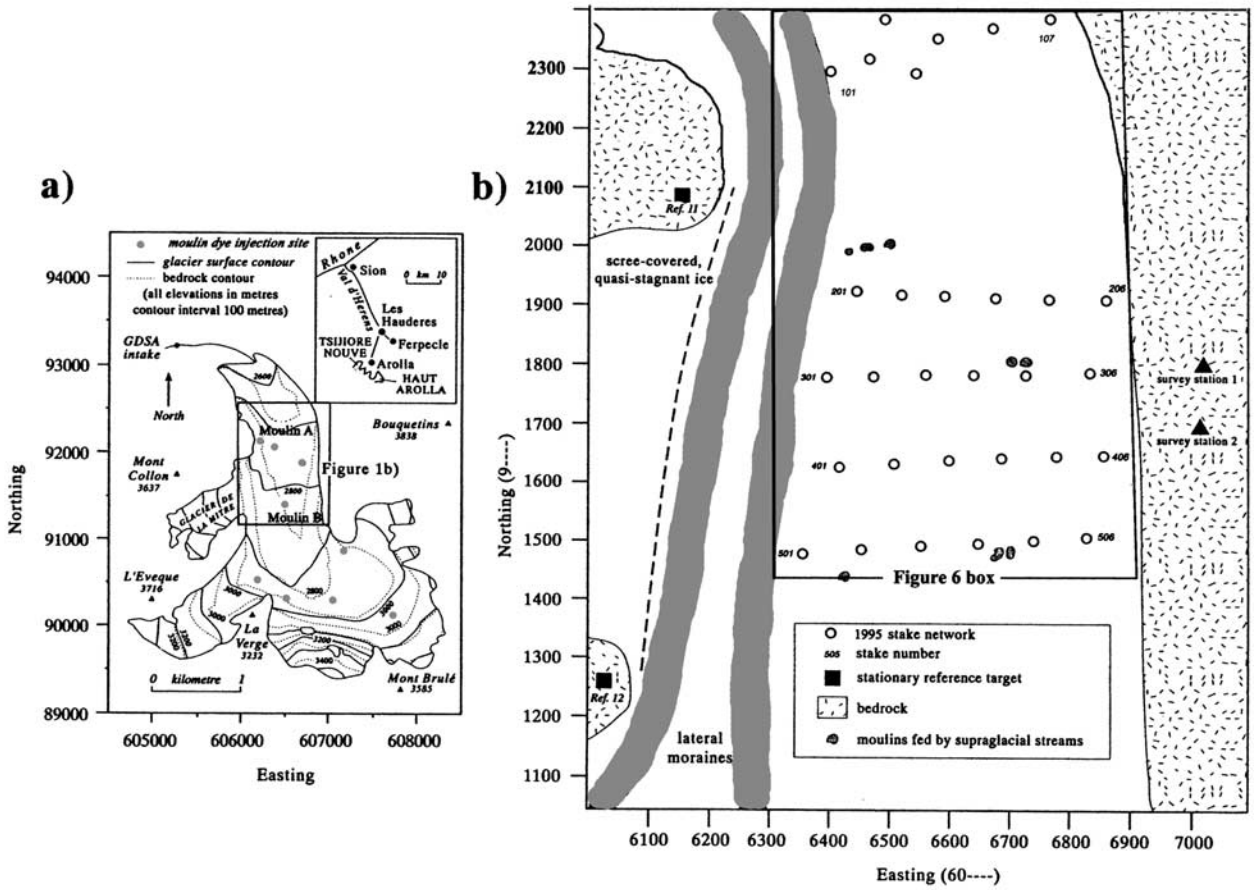

Figure 1. Location map of Haut Glacier d'Arolla, showing location of moulins used in dye tracing experiments and with inset of stake network.

glacier surface motion. However, the spatial scale over which surface motion changes may be representative of basal motion is many orders of magnitude greater than the scale over which discrete hydrological forcing occurs [*Balise and Raymond*, 1985; *Kamb and Echelmeyer*, 1986]. Across large spatial scales, hydrological forcings will vary in magnitude and phase across the glacier. Forcings will be applied locally over channels and heterogeneously over distributed drainage systems. Somehow the glacier integrates these forcings to produce a flow response over spatial scales of several ice thicknesses. *Iken and Truffer* [1997] suggested that intraannual changes in the spatial patterns and form of subglacial drainage conditions beneath the tongue of Findelengletscher, Switzerland, may have been the cause of intraannual variations in patterns of surface motion. *Hanson et al.* [1998] monitored changes in diurnal phase relationships between local water pressures and surface velocities on the tongue of Storglaciären, Sweden. They showed that as the melt season progressed, (1) surface speeds became more spatially coherent and (2) the timing of surface velocity increases changed from preceding the onset of local water pressure rise to becoming more in phase with the diurnal water pressure cycle. They suggested that as the drainage system evolves throughout the melt season, it becomes more integrated and coherent and that the flow response to hydrological forcing acts more like the theoretical models of glacier sliding. However, the process by which spatially incoherent subglacial drainage systems affect the spatial flow response of a glacier remains poorly understood. Through the analysis of field measurements we aim to understand how temporal and spatial changes in drainage system morphology throughout a melt season impacts upon a glacier's response to hydrological forcing over spatial scales typically used in glacier flow models, i.e., of the order of ice thickness. This work therefore contributes toward the goal of developing fully coupled, time-dependent, hydrological/ice flow models.

2. Field Site and Methods

[3] Haut Glacier d'Arolla is located above the village of Arolla at the head of the Val d'Hérens, Valais, Switzerland (Figure 1). The glacier consists of a 2.2-km-long, south-north trending tongue, ~750–800 m wide, fed by two separate firn basins. The glacier snout lies at an elevation of 2560 m. The main eastern basin rises to 3500 m and the western tributary basin rises to 3325 m. Total glacier length along the centerline of the main flow unit is ~4 km and the area of the glacier is 6.33 km^2. The glacier has been the subject of an integrated study of glacier hydrology and meltwater quality which has led to a detailed understanding

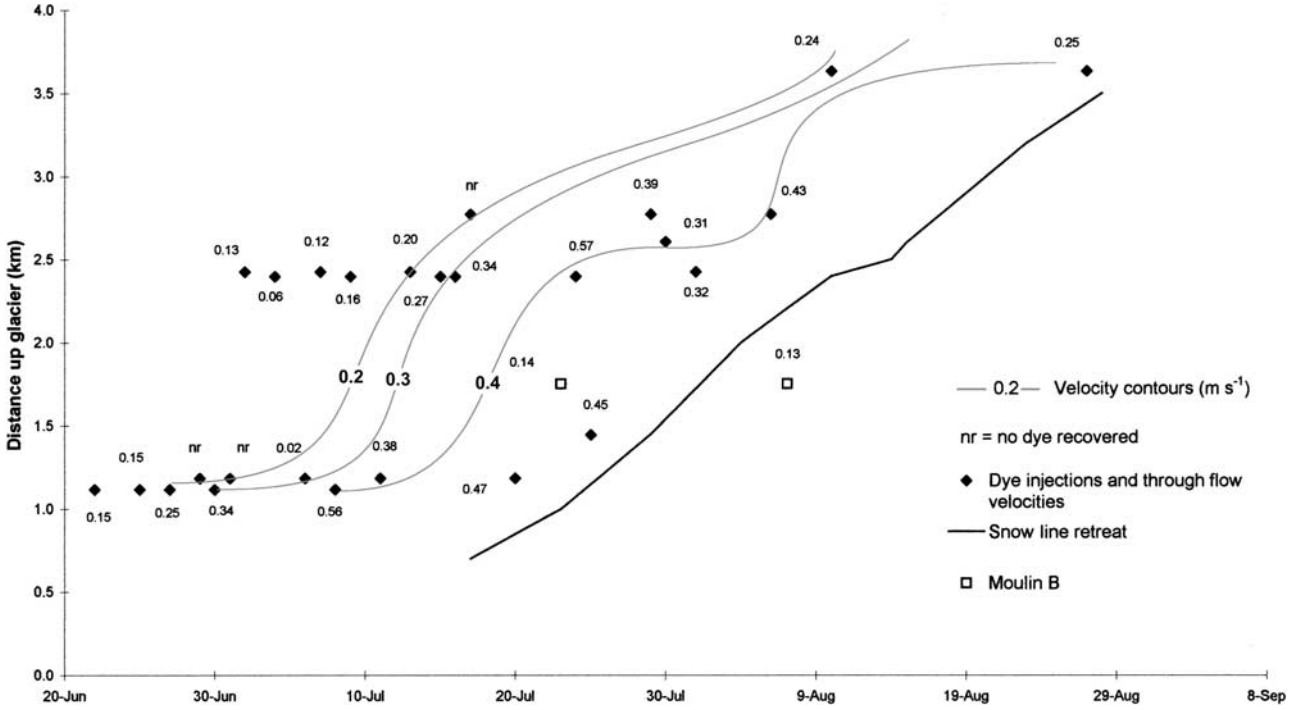

Figure 2. Time-space variation in dye travel time during the 1995 melt season. Approximate position of snow line is indicated.

of how the subglacial drainage system varies in space and time [*Richards et al.*, 1996].

2.1. Dye Tracing Experiments

[4] The techniques of dye tracing are well established, and the methods used at Haut Glacier d'Arolla are summarized elsewhere [*Sharp et al.*, 1993; *Nienow et al.*, 1998]. Dye tracing experiments have been used to investigate the structure of subglacial drainage systems, the hydraulic geometry of individual passageways [e.g., *Willis et al.*, 1990; *Fountain*, 1992; *Hock and Hooke*, 1993] and the spatial and temporal evolution of these systems [*Hock and Hooke*, 1993; *Nienow et al.*, 1998]. During the 1995 melt season, 30 dye tracer tests were carried out from nine moulins distributed widely across the glacier (Figure 1). At all nine sites the tests were initiated prior to removal of the snowpack and, where possible, continued until the mean through flow velocity from a given injection site to the snout exceeded 0.4 m s^{-1}. Through flow velocities of >0.4 m s^{-1} indicate that a tracer has been routed entirely via an efficient channelized drainage system [*Burkimsher*, 1983].

2.2. Glacier Motion Surveys

[5] Surface motion was recorded across a large area of the glacier tongue (Figure 1). Ice thicknesses across the study area ranged from ~40 m, ~50 m from the glacier margins, to ~130 m in the valley center. Glacier surface motion was determined from daily surveys of prisms mounted on stakes drilled into the glacier surface. *Sharp et al.* [1993] predicted that over most of the glacier, two main preferential drainage axes (PDAs) dominate the subglacial drainage network. Water level variations within boreholes drilled in the region of the eastern PDA confirmed this prediction by suggesting that late in the melt season a subglacial channel is present within a more widespread distributed drainage system [*Hubbard et al.*, 1995]. The channel flows along the center of a variable pressure axis (VPA) some tens of meters wide. In mid-June 1995 a dense array of 24 velocity stakes was established, centered on this area ~1400 m from the glacier snout (Figure 1). Surface strain rates were calculated from the deformation of strain triangles formed by these staggered rows of motion stakes [*Ramsay*, 1967]. A further row of seven stakes was established in a transverse profile ~600 m closer to the glacier snout. Full details of survey setup, strain rate measurements, and errors can be found elsewhere [*Mair et al.*, 2001].

2.3. Bulk Discharge

[6] Bulk meltwater discharge was measured automatically throughout the melt season at the Grande Dixence S.A. (GDSA)(hydroelectric power company) gauging station situated ~1.5 km down stream from the glacier snout (Figure 1).

3. Results

3.1. Dye Breakthrough Curve Characteristics

[7] Figure 2 presents the 1995 tracer results. The through flow velocity from a given site is plotted as a function of time and position along the length of the glacier. Where a velocity contour runs parallel to the time axis, velocities from locations that distance upglacier remain constant. Between approximately 30 June (J.D. 181) and 30 July (J.D. 211), the contours are steeply inclined from the lower left to the upper right, indicating that through flow velocities from a particular point were increasing through time and that the increase occurred progressively later in the summer

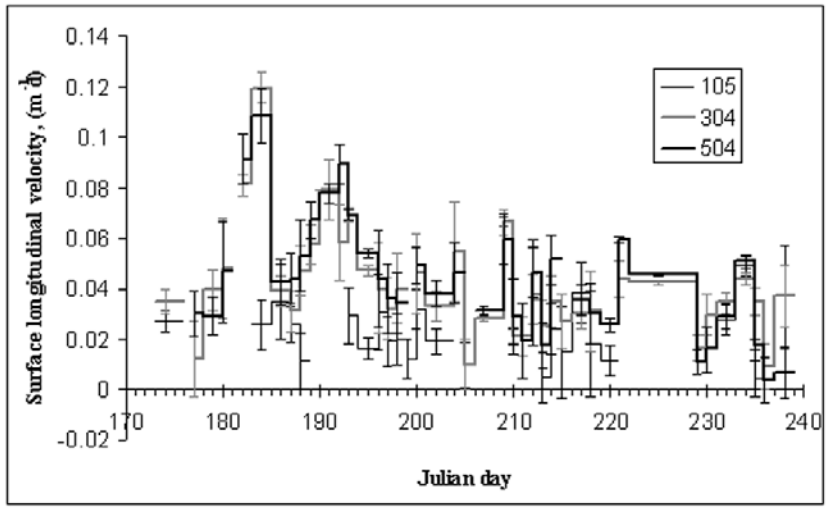

Figure 3. Surface longitudinal velocities for selected centerline stakes plotted against time throughout the 1995 melt season (error bars shown).

with increasing distance up glacier. Similar behavior was observed in 1989–1991 and was interpreted to be the result of transformation of the drainage system from distributed to channelized in character [*Nienow et al.*, 1998].

3.2. Glacier Surface Motion and Bulk Discharge

[8] The temporal pattern of centerline surface motion throughout the 1995 melt season (Figures 3 and 4) shows the following features: (1) an approximate threefold increase in velocity across most of the glacier tongue which peaked between 2 and 4 July (J.D. 183 and J.D. 185); (2) an approximate twofold velocity increase which peaked between 10 and 14 July (J.D. 191 and J.D. 195); (3) significant surface uplift that precedes peak longitudinal velocity by a day during speed up events; and (4) higher frequency variations in surface velocity after about 14 July (J.D. 195).

[9] Comparison of these data with the bulk discharge hydrograph (Figure 5) shows that (1) the first velocity event occurred during a rapid increase in bulk discharge, that began approximately 27 June (J.D. 178) and peaked on 4 July (J.D. 185); (2) the second velocity event occurred during a second period of increasing discharge between 6 July (J.D. 187) and 14 July (J.D. 195); (3) the reduction in velocity which followed each of these two periods, i.e., after 4 July (J.D. 185) and after 14 July (J.D. 195), coincided with reductions in discharge; and (4) between 19 and 22 July (J.D. 200 and J.D. 203) bulk discharge again increased rapidly, however, on this occasion the increase was associated with no significant or widespread increase in surface velocity.

3.3. Spatial Pattern of Glacier Surface Motion

[10] Spatial patterns of surface longitudinal motion across the glacier tongue are shown for the annual time period, 1994–1995, and for six periods between 25 June and 23 July (J.D. 176 and J.D. 204; Figures 6a–6g). Longitudinal surface strain rates for the same six periods are also shown (Figures 7a–7f). Poor surveying weather (particularly from

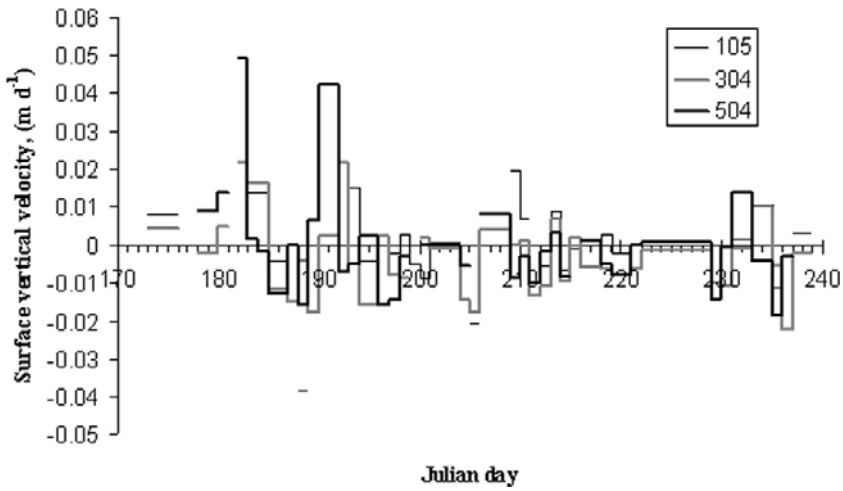

Figure 4. Surface vertical velocities for selected centerline stakes plotted against time throughout the 1995 melt season (measurements errors typically ±0.015 m d^{-1}).

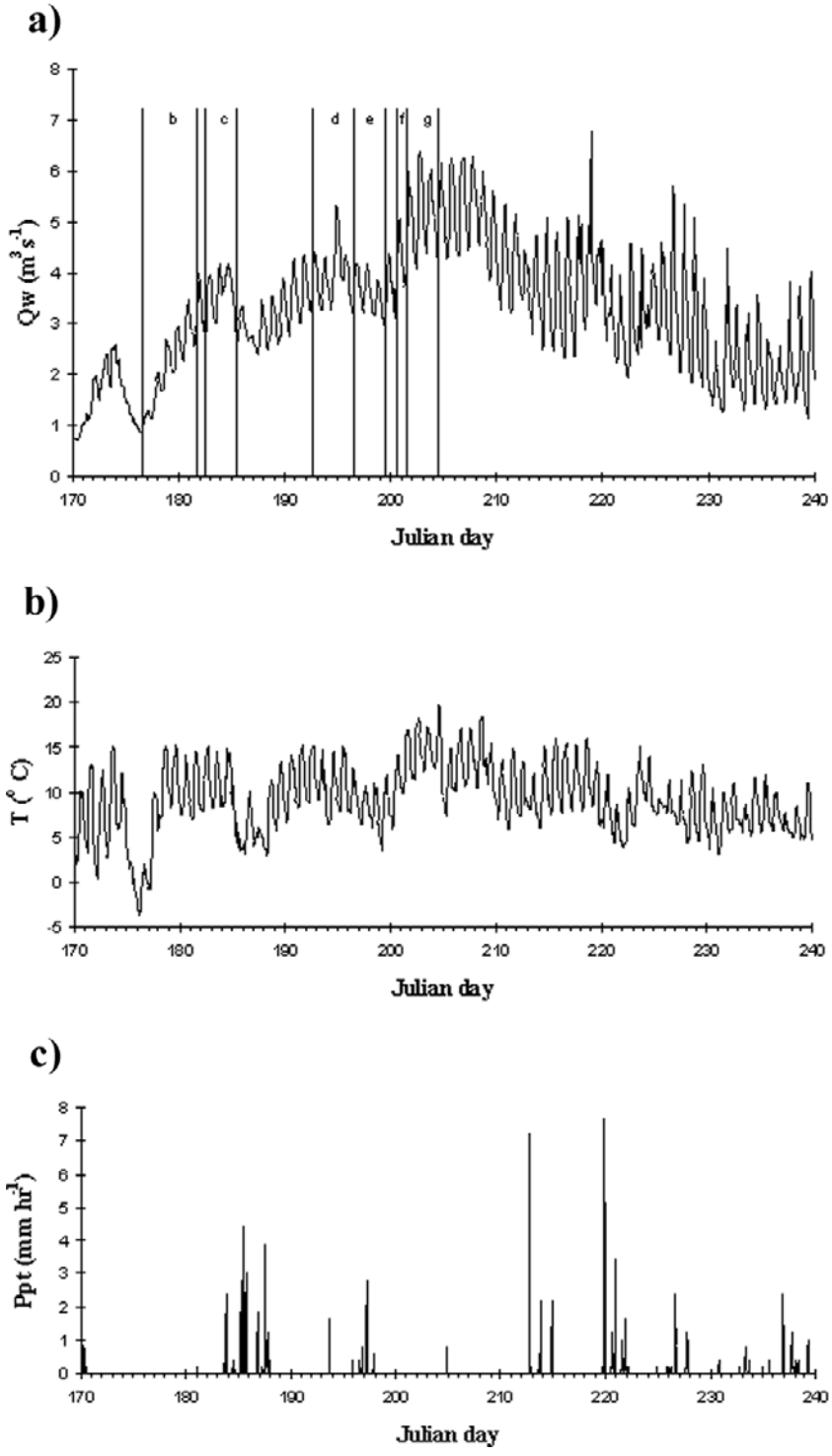

Figure 5. (a) GDSA bulk discharge hydrograph, 1995 melt season. Time periods over which spatial patterns of surface velocity were measured (Figure 6) are shown. (b) Air temperature measured at Bricola weather station, ~10 km northeast of Haut Glacier d'Arolla but at approximately the same elevation as the glacier terminus. (c) Precipitation measured at Bricola weather station.

5 to 9 July, J.D. 186–190) prohibited a continuous record of surface velocity across the entire study area. However, the periods shown all have good spatial coverage of velocity measurements, and they match closely with distinct episodes on the bulk discharge hydrograph (Figure 5a). The periods 1–4 July (J.D. 182–185), 11–15 July (J.D. 192–196), and 19–20 July (J.D. 200–201) correspond with the three main periods of increasing bulk discharge (see Figures 5, 6c, 6d, and 6f, respectively). The periods 25–30 June (J.D. 176–181), 15–18 July (J.D. 196–199), and 20–23 July (J.D. 201–204) correspond closely with periods before, between, and after bulk discharge increases (see

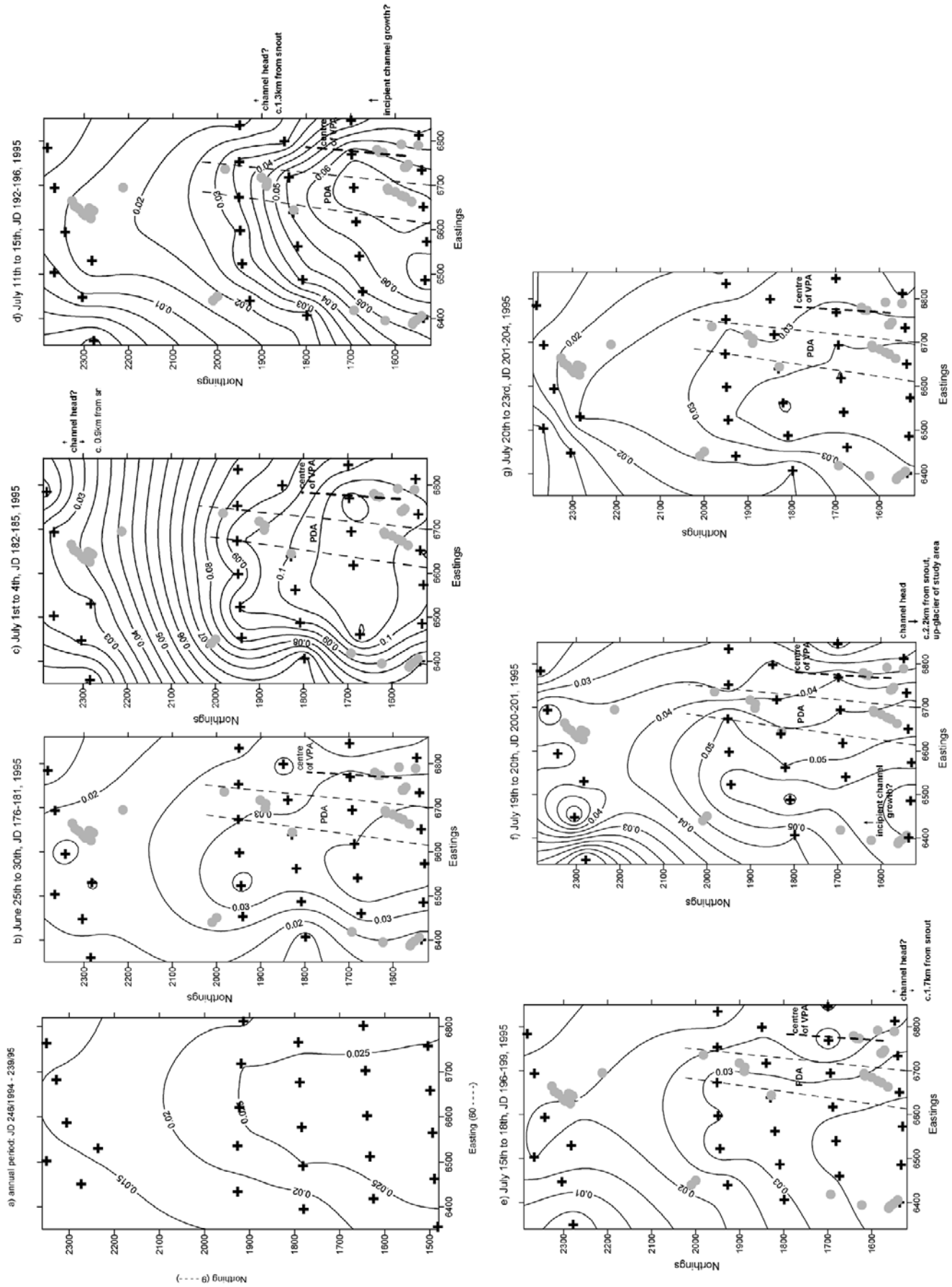
a) annual period: JD 248/1994 - 239/95
b) June 25th to 30th, JD 176-181, 1995
c) July 1st to 4th, JD 182-185, 1995
d) July 11th to 15th, JD 192-196, 1995
e) July 15th to 18th, JD 196-199, 1995
f) July 19th to 20th, JD 200-201, 1995
g) July 20th to 23rd, JD 201-204, 1995
Northings
Eastings
Easting (60 - - - -)
Northing (9 - - - -)
centre of VPA
PDA
channel head?
c.1.3km from snout
incipient channel growth?
c.1.7km from snout
c.2.2km from snout, up-glacier of study area
incipient channel growth?

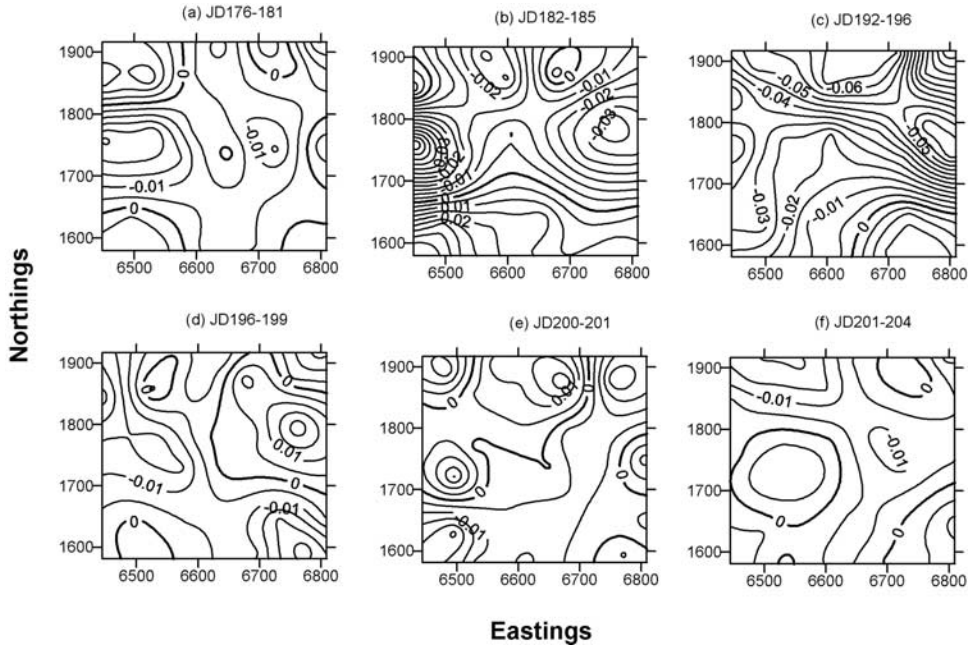

Figure 7. Spatial patterns of surface longitudinal strain rates (yr^{-1}) across the strain triangle network for each of the six selected time periods during the 1995 melt season (see Figures 5 and 6b–g). Measurement error is $\sim$0.1 yr^{-1}. Much of the spatial variation, particularly in Figures 7a, 7d, 7e, and 7f, may therefore be a consequence of errors.

Figures 5a, 6b, 6e, and 6g, respectively). Transverse velocities were considered insignificant since they were typically smaller than measurement errors.

4. Interpretation of Dye Tracing Results

4.1. Temporal Evolution of Subglacial Drainage System

[11] The dye tracing data can be used to determine the timing of the transition between distributed and channelized drainage across the study area. If it is assumed that a through flow velocity of $\sim$0.4 m s^{-1} indicates flow through a fully channelized drainage system, the point at which through flow velocities from a given location attain this value can be taken as evidence that the up-glacier limit of the channelized system has reached that location. Using this assumption, Figure 2 suggests that on 10 July (J.D. 191), the channel head was in the vicinity of 1.1 km from the glacier snout ($\sim$92100N). By 8 August (J.D. 220) the channel head had reached a point $\sim$2.8 km up glacier from the glacier snout ($\sim$90400N). This equates to a mean rate of channel evolution of $\sim$60 m d^{-1}, a similar rate to that observed in 1990 [*Nienow et al.*, 1998]. Locally, incipient channel growth was probably directed down glacier from individual moulins [*Nienow et al.*, 1998] as the thinning and saturation of the snow cover continually affected new moulins and crevasses and subjected them to increasingly peaked diurnal inputs of surface meltwater. Water flow velocities will reach $\sim$0.4 m s^{-1} only when the incipient channel connects to the major channel system that extends to the glacier snout. Figure 2 suggests that the moulins located at the up-glacier edge of the study area ($\sim$1.7 km from the glacier snout, $\sim$91500N, Figure 1) would have connected to the main channelized system by approximately 19 July (J.D. 200). Thus incipient channel development probably occurred within the study area after the first discharge increase, during the second and before the third. In contrast to the 1990 and 1991 results, the position of the inferred channel head does not match that of the transient snow line although the trend closely mirrors the snow line's movement up glacier (Figure 2). This result is discussed further in Appendix A.

4.2. Spatial Pattern of Evolution of Subglacial Drainage System

[12] Insufficient dye tracing experiments were conducted during the 1995 melt season to determine the spatial structure of the evolution of channelized drainage (for example, by following the rules for drainage system reconstruction outlined in Table I of *Sharp et al.* [1993]). There is evidence from other temperate valley glaciers (e.g., Findelengletscher, Switzerland [*Iken and Truffer*, 1997], and Storglaciären, Sweden [*Hooke et al.*, 1989]) that quite different subglacial drainage systems may evolve from one year to the next. However, there are enough consistencies between our 1995 dye tracing results and results from the

Figure 6. (opposite) Spatial patterns of surface longitudinal motion across the glacier tongue for annual time period (1994–1995) and selected time periods during 1995 melt season (see Figure 5). Velocity contours are in m d^{-1}. Location of velocity stakes (crosses), moulins (shaded circles), the eastern PDA, and the center of VPA are shown. Inferred location and status of channel development are indicated.

far more extensive dye tracing programs of 1990 and 1991 [*Nienow et al.*, 1998] to indicate that at Haut Glacier d'Arolla the spatial pattern of subglacial channel evolution would be similar for each year. In addition, results from water level/pressure measurements within extensive borehole arrays over several years (1992–1995) suggest that subglacial drainage axes tend to form in approximately the same location each year [*Gordon*, 1996]. It is therefore likely that channelized drainage evolved along the eastern VPA/PDA. The center of the measured VPA lies close to the predicted PDA (Figures 6b–6g). Moulins, which mark the points of entry of surface streams into the glacier, tend to be clustered along the line of the major subglacial drainage pathways (Figures 6b–6g). The inferred status of channel development is shown for each time period in Figures 6b–6g, based upon analysis of Figure 2. From the above interpretation of the dye tracing experiments it seems evident that the majority of moulins in at least the lower 3 km of the glacier became connected to an efficient channelized drainage system during the course of the 1995 melt season. However, dye injections at moulin B (located 1.75 km up glacier, Figure 1) suggest that it remained hydraulically isolated from the channelized drainage system. Tests undertaken on 23 July (J.D. 204) and 7 August (J.D. 219) resulted in through flow velocities of $\sim$0.14 m s^{-1}, while tests from sites farther up glacier were generating through flow velocities of between 0.31 and 0.57 m s^{-1} (Figure 2). The results from moulin B are consistent with those from tracing work in 1990 and 1991 which indicate that within the lower glacier some moulins are connected to a residual section of inefficient distributed drainage that persisted in interchannel areas throughout the melt season (P. Nienow et al., The spatial extent of channelised and distributed subglacial drainage systems: Implications for ice dynamics and subglacial sediment evacuation, submitted to *Hydrolical Processes,* 2001).

5. EOF Analysis of Surface Velocity Fields

[13] Spatial patterns of surface longitudinal velocity for periods throughout the 1995 melt season were analyzed in terms of empirical orthogonal functions (EOFs). A schematic cartoon, illustrating the basic concepts of the analysis, is included to help explain the following summary (Figure 8). The method is reviewed and explained in full by *Peixoto and Oort* [1992, pp. 67–69, Appendix B, p. 492]. Since its introduction in the atmospheric sciences in the 1950s, this type of analysis has also been widely used in hydrology, oceanography, and solid earth geophysics. It has not been used previously to study temporal and spatial patterns of glacier motion. The measured surface velocities from 31 stakes over 31 days between 25 June and 6 August (J.D. 176 and J.D. 218) are organized into a matrix where each row represents a single stake and each column represents a single day (gaps in the velocity records of some stakes are filled with spatially interpolated values). The square of this matrix is then decomposed into 31 normalized eigenvectors and 31 eigenvalues. When the elements of the individual eigenvectors are mapped to the 31 stake locations on the glacier, they define distinct spatial modes (or EOFs) of surface velocity (Figure 9). The observed spatial velocity pattern, at any given time, can be exactly reconstructed by weighting each of the linearly independent EOFs (by multiplying it by its coefficient) and adding them together. The time series of the coefficients of each mode (Figure 10) indicate the relative strength and sign (positive or negative) of each mode at any given time. The eigenvalues associated with each EOF, divided by the sum of all the eigenvalues, indicate the proportion of the total variance in velocity patterns, throughout the melt season, accounted for by each EOF. The EOF modes are arranged in decreasing order according to the percentage of variance explained by them. Thus the EOF analysis breaks down the data into a set of linearly independent modes, each of which accounts for a certain percentage of the total spatial and temporal variance within the original data.

[14] Unlike most other orthogonal representations, the EOFs are derived directly from the data themselves rather than being a predetermined orthogonal set of analytical functions (e.g., Fourier analysis). Furthermore, the first few EOF modes usually explain a much higher fraction of the total variance than the same number of other orthogonal functions. Thus fewer empirical functions are usually required to explain the same amount of variance in the data. EOF analysis and principal components analysis (PCA) [*Johnston*, 1980] both solve for the eigenvectors and eigenvalues of the same correlation matrix. Although the terms ''principal component'' and ''EOF'' describe the same orthogonal functions, the results are used differently. PCA involves correlating the individual time series at each original grid point with the coefficient time series of each principal component (or EOF). The results are then clustered according to which principal component correlates best with each grid point. Some points will correlate best with principal component 1, and others will correlate best with principal component 2, etc. In PCA, the spatial plots of the various principal components (or EOFs) are not analyzed. In the EOF analysis presented here, we look at the spatial patterns of the different EOF modes to determine whether the patterns of the most dominant modes can be interpreted physically. The EOF modes which account for a large fraction of the variance are, in general, considered to be physically meaningful, while the higher-order EOF modes represent minor features and smaller-scale fluctuations and are most likely due to sampling and measurement errors.

[15] Without de-trending the original data, a contour plot of the most dominant EOF mode shows a regular parabolic pattern (Figure 9a). This pattern is virtually identical to the long-term mean surface velocity pattern (Figure 6a) and is indicative of the background low-frequency variability due to ice deformation and long-term, average basal motion. In the results presented here, the input data have been temporally de-trended before analysis. This effectively removes the background, long-term pattern due to ice deformation and average basal motion, which otherwise accounts for over 90% of all spatial variation in surface velocity throughout the melt season. De-trending the data makes it easier to identify spatial patterns of surface velocity which are statistically significant but act over shorter timescales. EOFs 1 and 2 (Figures 9b and 9c) account for 74.33% and

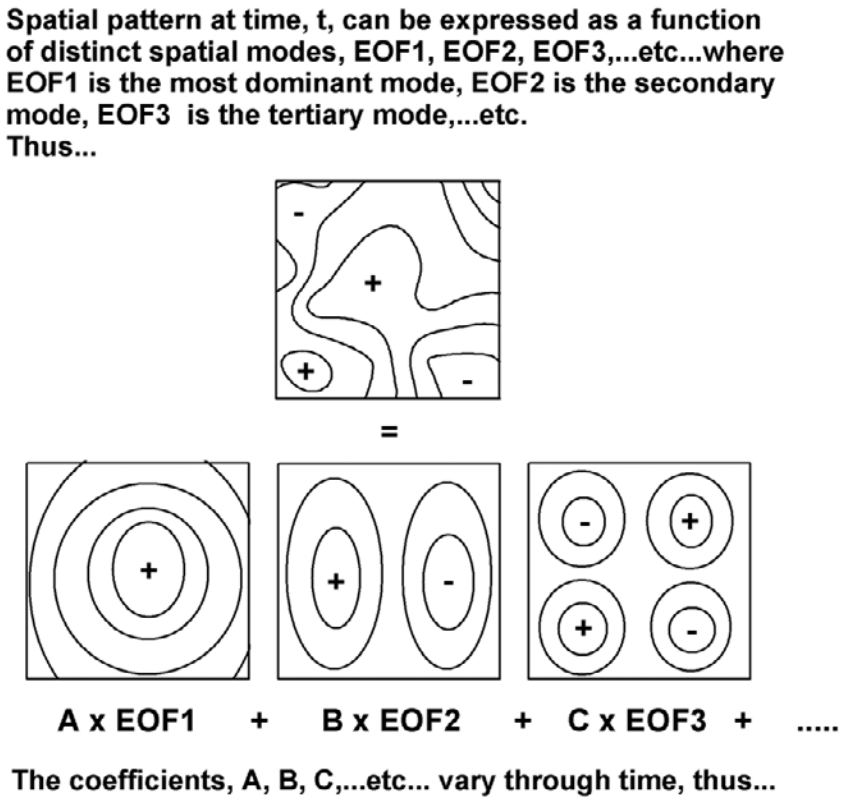

Figure 8. Schematic cartoon illustrating the essential elements of the empirical orthogonal function (EOF) analysis.

14.62%, respectively, of the remaining spatial variation in velocity throughout the melt season. The remaining 29 modes between them account for just 11.05% of the spatial variation and for this reason they are not considered here. The spatial patterns of the resulting de-trended modes 1 and 2 are therefore assumed to be primarily the result of shorter-term hydraulic basal forcing.

[16] To aid our interpretation of the causes of the temporal variations in measured motion fields, the two most significant modes may be physically interpreted as follows. EOF 1 (Figure 9b) still shares many of the characteristics of the background deformation motion field (Figure 9a), i.e., surface velocity generally increases up glacier and toward the centerline. This suggests a fairly uniform basal forcing across the glacier. If effective subglacial water pressures are uniform across the study area, then variations in basal motion will be largely driven by variations in the driving stress. Basal motion therefore adds to the velocity pattern caused by ice deformation rather than replacing it. However, there is a high eigenvector anomaly in the southeast of the

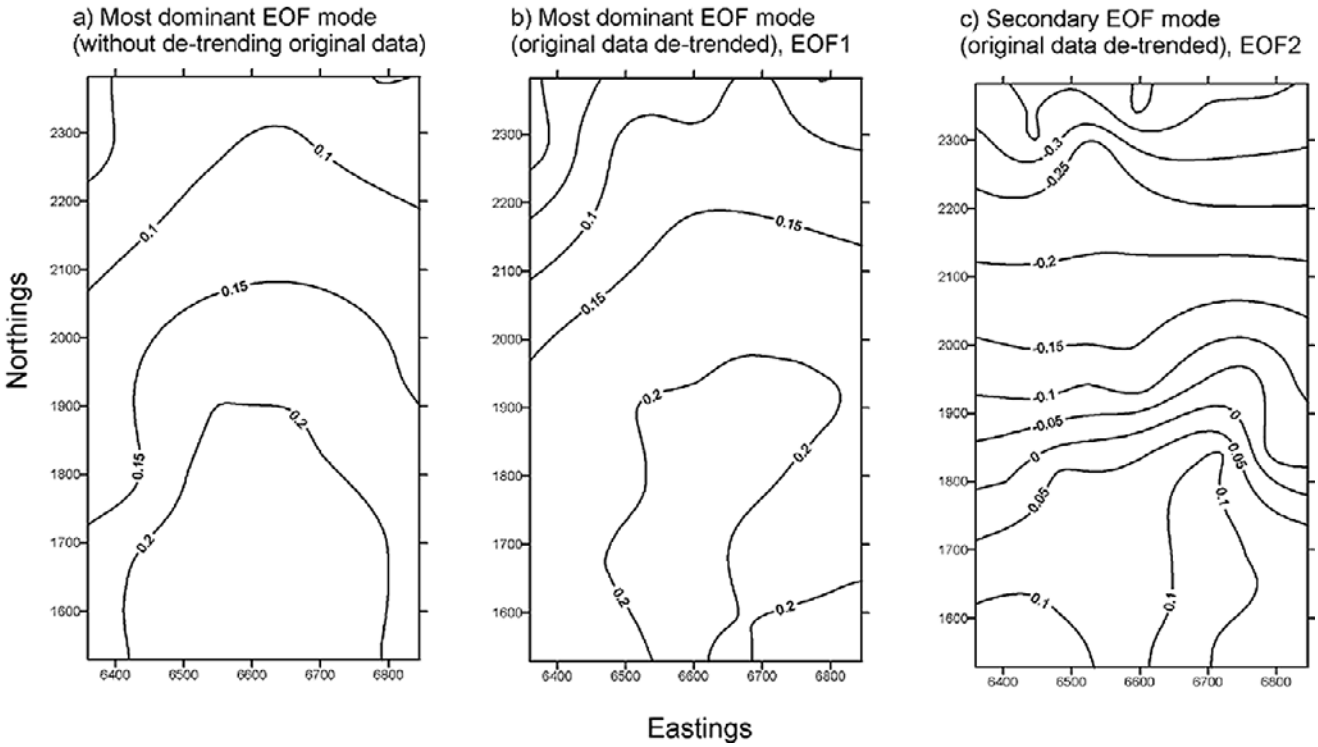

Figure 9. Eigenvector modes from the empirical orthogonal function (EOF) analysis of spatial patterns of surface velocity throughout the 1995 melt season. Higher (lower) values indicative of higher (lower) surface velocity.

study area where a cluster of moulins are aligned along the eastern PDA. This is likely to indicate a concentration of high hydrological forcing in this area. EOF 2 (Figure 9c) shows a positive eigenvector anomaly elongated down glacier below the moulins precisely overlying the upper eastern PDA and in the southwestern corner of the study area. EOF 2 is therefore interpreted as representing the glacier flow pattern resulting from a localized hydrological

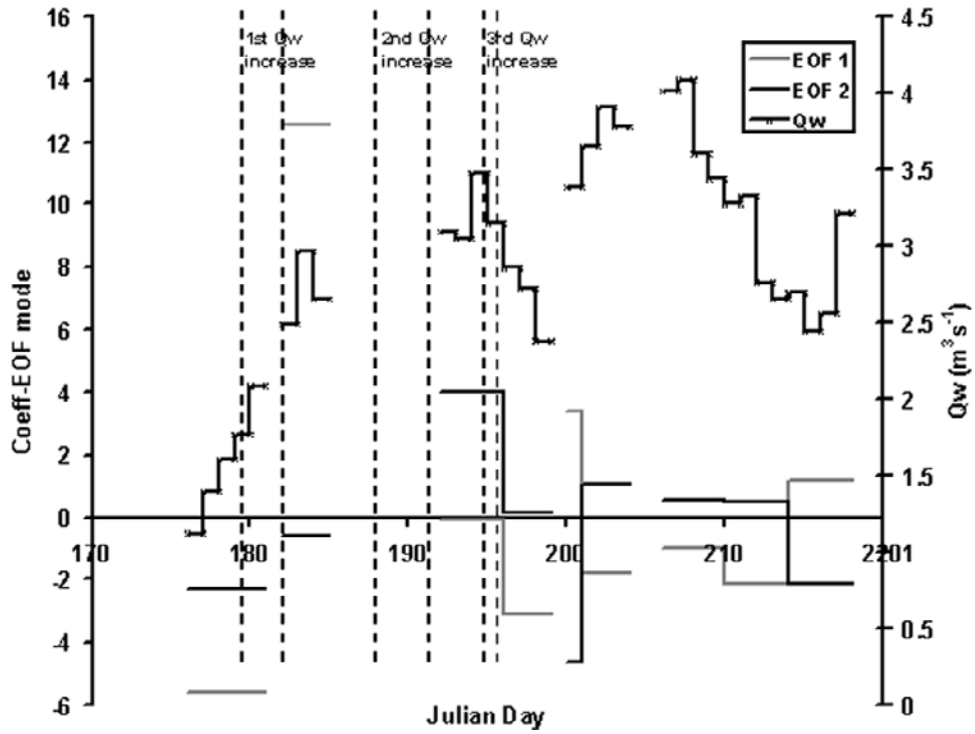

Figure 10. Coefficients of the EOF modes and average daily bulk discharge, Qw, for selected time intervals during the 1995 melt season.

forcing along an incipient channel within the eastern subglacial drainage axis and possibly identifying the response to forcing close to the western PDA.

6. Interpretation of Glacier Motion Variations

[17] During the three intervals when both diurnal peak and minimum bulk discharges increased over periods of several days, both the magnitudes and spatial patterns of glacier surface velocity were appreciably different from the annual flow regime (see Figures 6a, 6c, 6d and 6f). During the first period of increasing bulk discharge (1–4 July, J.D. 182–185), glacier surface velocity increased everywhere. High bulk discharge occurred as a result of a combination of high melt rates (caused by a sustained period of high air temperatures; Figure 5b) and high precipitation (Figure 5c). The region of highest velocity was displaced east of the flow centerline (Figure 6c), suggesting a focus of basal forcing in the area immediately down glacier of several moulins which lie along the eastern drainage axis. Longitudinal strain rates show a widespread pattern of extending flow farther up glacier and highly compressive flow farther down glacier (Figure 7b). Such a pattern indicates that much of the resistance to flow within the study area may come from slower moving ice down glacier rather than from basal drag. The coefficient of EOF 1 was more dominant than at any other time during the season (Figure 10), suggesting widespread basal forcing across the glacier tongue. The dye tracing suggests that at this early stage of the melt season, most of the glacier tongue was underlain by a distributed drainage system. Theory suggests that distributed drainage systems display a direct relationship between discharge and water pressure [*Walder*, 1986; *Kamb*, 1987]. Thus high surface velocities were most likely a consequence of increased basal motion due to high subglacial water pressures caused by rapidly increasing water discharge through a distributed drainage system. High water pressures may cause widespread bed separation and reduced basal drag. This may explain higher rates of surface uplift occurring farther up glacier (Figure 4), closer to the water input point below the moulins.

[18] During the second period of increasing discharge (11–15 July, J.D. 192–196) surface velocity increased significantly across most of the up glacier half of the study area (Figure 6d). This increase in bulk discharge was primarily a result of high melt rates, again caused by a sustained period of high air temperatures (Figure 5b). Longitudinal strain rates show that the pattern of extending flow up glacier and compressive flow farther down glacier is now concentrated within the eastern half of the study area (Figure 7c). The coefficient of EOF 2 reached its most positive value of the entire melt season and the coefficient of EOF 1 was very close to zero (Figure 10). This indicates that hydrological forcing had become more localized over the up-glacier sections of the PDAs, where incipient channel growth was likely to have developed. This pattern is consistent with the inferred status of channel evolution by this time period. The main channel head is likely to have migrated to $\sim$1.3 km from the snout, as far as the moulins located in the down glacier half of the main stake network (i.e., about GR6690E 1880N, Figure 6d), while incipient channel growth is likely to have begun progressing down-glacier from the moulins farther up glacier (i.e., about GR6690E 1600N). Localized areas of very high water pressure were likely to have developed in the incipient channel since it had not connected to the main channel and was therefore blocked at its downstream end by inefficient distributed drainage. Basal forcing was likely to be strong enough to promote enhanced basal motion and therefore high surface velocities in this area. It is probable that high water pressures in the incipient channel would have eventually driven a connection to the main channel farther downstream, thereby reducing water pressure and the velocity response, but this is not evident from the time-averaged data.

[19] During the third period of increasing discharge (19–20 July, J.D. 200–201) surface velocity increased only slightly across most of the study area (Figure 6f). This increase in bulk discharge was driven by high surface melt as air temperatures approached the highest of the entire summer (Figure 5b). The smallest increase in velocity was toward the east. Longitudinal strain rates have generally lower magnitudes than during the previous two periods of discharge increase and so the more complex spatial pattern may be largely a consequence of measurement errors (Figure 7e). The coefficient of EOF 2 becomes more strongly negative (Figure 10). As suggested above, high water pressures in the incipient channel would have already driven a connection to the main channel system and the channel head is likely to have migrated up glacier to a location above the study area. Higher discharges were therefore able to drain at low water pressures through this efficient subglacial channel and basal motion was unaffected. Although at peak discharge water pressures in the main channel and surrounding areas can reach values in excess of ice overburden pressure [*Hubbard et al.*, 1995], this is a short-lived, transient effect. Over a period of hours and days the effect of the channel is to cause lower water pressures. This occurs since (1) water pressures are lowered as water flux increases within the channel, following *Röthlisberger*'s [1972] model of glacier hydrology and (2) the water pressure gradient between higher-pressure distributed areas adjacent to the channel and the low-pressure channel causes drainage to be concentrated toward the channel. Thus although bulk subglacial discharge increased during this time period, water fluxes through areas of persistent distributed drainage system down glacier of the channel head were likely to be reduced. If water pressures in down-glacier areas of distributed drainage do not become high enough, the basal motion response will be minimal (e.g., following *Iken* [1981]). Velocity increases are higher west of the glacier center, close to where the western PDA was predicted [*Sharp et al.*, 1993]. This may reflect localized basal forcing within incipient channels developing down glacier of the more westerly moulins. The western PDA drains a much smaller catchment than the eastern PDA [*Sharp et al.*, 1993], so the onset and evolution of channel evolution would be expected to be later than farther east.

[20] Before, between, and after these discharge increases surface velocity patterns resemble the annual flow regime which is dominated by ice deformation (see Figures 6a, 6b, 6e, and 6g). Hydrology only causes a velocity response when discharge is rising and when the drainage system is not fully channelized. After the third increase in bulk discharge the magnitudes of coefficients are generally low,

and no mode dominates over another. This pattern is consistent with the timing of the development of fully channelized subglacial drainage within the study area.

7. Discussion

[21] Because of longitudinal and transverse coupling within the ice, significant increases in basal motion will only affect surface velocity across the entire glacier when a rapid and sustained increase in meltwater inputs causes high basal water pressures and low basal drag over a very large area of the bed. Such events are most likely at the start of the melt season when rapidly increasing melt rates coincide with a hydraulically inefficient drainage system. Force budget analysis of glacier motion during a major motion event at the start of the 1994 melt season [*Mair et al.*, 2001] suggested that fast flow (i.e., surface velocity 400–500% higher than annual average velocity) was dependent upon the reduction of basal drag and the removal of areas of high drag from areas of length scales of the order of at least four or five ice thicknesses. Although a full force budget analysis of glacier motion throughout the 1995 melt season is out with the scope of this paper, the data and analysis presented here would appear to be consistent with such an interpretation. During the first rapid increase in bulk discharge in 1995 longitudinal velocity was in excess of 0.1 m d^{-1} over a very large region (at least ~400 m × 300 m, Figure 6c) and the transition from extending to compressive longitudinal flow spanned the entire study area (Figure 7b). Where basal forcings are more localized and separated by distances greater than a few ice thicknesses, the velocity response will be much smaller (e.g., during the second discharge increase, Figure 6d) and the extension-compression strain rate pattern less widespread (Figure 7c). As the melt season progresses, the evolution of a channel will reduce the mean subglacial water pressure response to rising discharge within the channel and will decrease water flux in surrounding distributed drainage areas. Both these effects will prevent water pressures from rising high enough to promote enhanced basal motion. Although a subglacial channel is likely to be just a few meters wide, borehole experiments indicate that the presence of a channel may influence the water pressure response to variable discharge within the adjacent distributed drainage system up to 70 m laterally from the center of the channel [*Hubbard et al.*, 1995]. Thus the presence of a channel may have a direct and/or indirect effect on water pressures across a ~140-m-wide axis running through the eastern half of the study area, i.e., about a third of the width of the study area. If it is assumed that during periods of rising discharge little or no change in surface velocity is indicative of minimal basal forcing then the pattern of surface motion during the third rapid increase in bulk discharge (19–20 July, J.D. 200–201, Figure 6f) appears to be consistent with this interpretation. Surface velocities across a band ~100–150 m wide in the region of the inferred channel increased only slightly compared with the increase in more westerly areas. Furthermore, some of the increase in velocity over the channel axis may be due to increased deformation due to coupling to faster flowing ice to the west. It seems that over spatial scales of a few ice thicknesses, the form of the subglacial drainage system does modulate the glacier's spatial velocity response to rising discharge.

8. Conclusions

[22] The relationship between drainage system evolution, subglacial water pressures and glacier dynamics over spatial scales of several ice thicknesses is not straightforward. However, from the above results and interpretation, combined with extensive previous research of glacier hydrology and dynamics, the key components of the relationship between subglacial hydrology and glacier dynamics may be summarized as follows.

[23] As bulk discharge rises throughout the melt season, (1) subglacial drainage along PDAs evolves from a distributed system to incipient channels to a fully channelized drainage system; (2) the percentage of bulk discharge flowing through the channelized system increases at the expense of discharge through the distributed drainage system; (3) the spatial extent of high water pressures in interchannel areas of distributed drainage decreases; (4) channelized drainage reduces mean subglacial water pressures along an axis of ~100–150 m width; (5) widespread high-velocity events occur when discharge rises and water pressures are increased across large areas of the bed, i.e., mainly within areas of distributed drainage but also within incipient channels; and (6) the magnitude, spatial extent, and frequency of glacier speed up events decreases.

[24] The EOF analysis clearly indicates that although variations in the local driving stress dominate spatial variation in surface velocity (e.g., Figure 9a), we can identify hydrologically induced flow patterns over spatial scales of a few ice thicknesses (EOFs 1 and 2, Figures 9b and 9c). The change in sign of the coefficient of EOF 2 between the second and third periods of increasing bulk discharge is indicative of the change in basal forcing along the drainage axis. Basal forcing along an incipient channel is minimal once it connects to the fully developed channelized system farther down glacier. *Hanson et al.* [1998, p. 367] stated that "current sliding laws do not explicitly recognize the possibility of temporal changes in coherence of the subglacial hydraulic system." They suggested that sliding laws that relate basal motion to local variables, such as basal shear stress and water pressure, ought to include a term describing the coherence of the hydraulic system. While this may improve existing sliding laws, a more quantitative relationship between temporal and spatial patterns of subglacial hydrology and glacier motion is not possible without more direct and extensive concurrent measurements of subglacial water pressure, basal sliding, bed deformation, internal ice deformation, and surface velocity. Even then, issues of scale and sampling will limit the general application of empirically derived relationships from such measurements and will necessitate the integration of results from hydrological and flow modeling experiments to constrain, confirm, and/or extrapolate our conclusions across larger spatial scales.

Appendix A: Channel Head Migration and the Position of the Transient Snow Line

[25] The assumption of previous research [*Richards et al.*, 1996; *Nienow et al.*, 1998], that the position of the

transient snow line is strongly associated with the up-glacier position of the channel head was not applicable to the 1995 melt season. However, the suggested mechanism for channel development may still apply. The snowfall during the winter of 1994/95 was the fourth largest in the last 60 years (Weissfluhjoch, Swiss Aalanche Srvice, unpublished data), so the retreat of the snow line during the melt season was atypically late. The results from 1995 suggest that if a snowpack is present well into the melt season, there may be time for (1) the development of more hydraulically efficient percolation of surface snowmelt to the base of the snowpack and (2) an efficient supraglacial drainage system to develop within a saturated layer of the snowpack at the snow-ice interface. Snow pits were dug immediately up glacier of snow covered moulins in early July 1995 and successfully located supraglacial streams at the snow-ice interface draining into the moulins. It may be that water from diurnal melting of surface snow was drained through the snowpack rapidly enough that these supraglacial streams developed diurnal meltwater discharge cycles. Such diurnal input cycles to the moulins may have been sufficient to destabilise the subglacial distributed drainage system and enable the ultimate development of subglacial channels (following *Kamb* [1987]). Thus if heavy snowfall during the spring creates a thick snowpack which persists well into the melt season, the development of channelized subglacial drainage may precede the snow line retreat.

[26] **Acknowledgments.** Our work was supported by Natural Environmental Research Council (NERC) Studentship GT4/93/6/P, NERC Fellowship GT3/93/AAPS/1, and NERC Grant GR3/8114. D.M. gratefully acknowledges the support of the Leverhulme Trust. Field assistance was provided by B. Hubbard and members of the Arolla Glaciology Project. We thank Grande Dixence SA, Y. Bams, V. Anzevui, and P. and B. Bournissen for logistical support. The comments of B. Hanson and two anonymous reviewers helped to improve this paper substantially.

References

Balise, M. J., and C. F. Raymond, Transfer of basal sliding variations to the surface of a linearly viscous glacier, *J. Glaciol.*, *31*, 308–318, 1985.

Boulton, G. S., and R. C. A. Hindmarsh, Sediment deformation beneath glaciers: rheology and geological consequences, *J. Geophys. Res.*, *92*, 9059–9082, 1987.

Burkimsher, M., Investigations of glacier hydrological systems using dye tracer techniques: Observations at Pasterzengletscher, Austria, *J. Glaciol.*, *29*, 403–416, 1983.

Fountain, A. G., Subglacial water flow inferred from stream measurements at South Cascade Glacier, Washington, U.S.A., *J. Glaciol.*, *38*, 51–64, 1992.

Fountain, A. G., Borehole water level variations and implications for the subglacial hydraulics of South Cascade Glacier, Washington State, U.S.A., *J. Glaciol.*, *40*, 293–304, 1994.

Gordon, S., Borehole-based investigations of subglacial hydrology, M.Sc. thesis, Univ. of Alberta, Edmonton, Alberta, Canada, 1996.

Gordon, S., M. Sharp, B. Hubbard, C. Smart, B. Ketterling, and I. Willis, Seasonal reorganisation of subglacial drainage system of Haut Glacier d'Arolla, Valais, Switzerland, inferred from measurements in boreholes, *Hydrol. Processes*, *12*, 105–133, 1998.

Hanson, B., R. L. Hooke, and E. M. Grace Jr., Short-term velocity and water-pressure variations down-glacier from a riegel, Storglaciären, Sweden, *J. Glaciol.*, *44*, 359–367, 1998.

Hock, R., and R. L. Hooke, Evolution of the internal drainage system in the lower part of the ablation area of Storglaciären, Sweden, *Geol. Soc. Am. Bull.*, *105*, 537–546, 1993.

Hooke, R. B., P. Calla, P. Holmund, M. Nilsson, and A. Stroeven, A 3 year record of seasonal variations in surface velocity, Storglaciären, Sweden, *J. Glaciol.*, *35*, 235–247, 1989.

Hubbard, B., M. Sharp, I. Willis, M. Nielsen, and C. Smart, Borehole water-level variations and the structure of the subglacial drainage system of Haut Glacier d'Arolla, Valais, Switzerland, *J. Glaciol.*, *41*, 572–583, 1995.

Humphrey, N. F., Coupling between water pressure and basal sliding in a linked-cavity hydraulic system, *IASH Publ.*, *170*, 105–119, 1987.

Iken, A., The effect of the subglacial water pressure on the sliding velocity of a glacier in an idealised numerical model, *J. Glaciol.*, *27*, 407–421, 1981.

Iken, A., and R. A. Bindschadler, Combined measurements of subglacial water pressure and surface velocity of the Findelengletscher, Switzerland: Conclusions about drainage system and sliding mechanism, *J. Glaciol.*, *32*, 101–119, 1986.

Iken, A., and M. Truffer, The relationship between subglacial water pressure and velocity of Findelengletscher, Switzerland, during its advance and retreat, *J. Glaciol*, *43*, 328–338, 1997.

Johnston, R. J., *Multivariate Statistical Analysis in Geography*, Addison-Wesley-Longman, Reading, Mass., 1980.

Kamb, W. B., Glacier surge mechanism based on linked cavity configuration of the basal water conduit system, *J. Geophys. Res.*, *92*, 9083–9100, 1987.

Kamb, W. B., and K. A. Echelmeyer, Stress-gradient coupling in Glacier flow, I, Longitudinal averaging of the influence of ice thickness and surface slope, *J. Glaciol.*, *32*, 267–284, 1986.

Lliboutry, L., Local friction laws for glaciers: a critical review and new openings, *J. Glaciol.*, *23*, 67–95, 1979.

Mair, D., P. Nienow, I. Willis, and M. Sharp, Spatial patterns of glacier motion during a high velocity event: Haut Glacier d'Arolla, Switzerland, *J. Glaciol.*, *47*, 9–20, 2001.

Nienow, P., M. Sharp, and I. Willis, Seasonal changes in the morphology of the subglacial drainage system, Haut Glacier d'Arolla, Switzerland, *Earth Surf. Processes Landforms*, *23*, 825–843, 1998.

Peixoto, J. P., and A. H. Oort, *Physics of Climate*, Am. Inst. of Phys., New York, 1992.

Ramsay, J. G., *Folding and Fracturing of Rocks*, McGraw-Hill, New York, 1967.

Richards, K. S., M. Sharp, N. Arnold, A. Gurnell, M. Clark, M. Tranter, P. Nienow, G. Brown, I. Willis, and W. Lawson, An integrated approach to modelling hydrology and water quality in glacierized catchments, *Hydrol. Processes*, *10*, 479–508, 1996.

Röthlisberger, H., Water in intra- and sub-glacial channels, *J. Glaciol.*, *11*, 177–203, 1972.

Sharp, M., K. Richards, I. Willis, N. Arnold, P. Nienow, W. Lawson, and J.-L. Tison, Geometry, bed topography and drainage system structure of the Haut Glacier d'Arolla, Switzerland, *Earth Surf. Processes Landforms*, *18*, 557–571, 1993.

Truffer, M., K. A. Echelmeyer, and W. D. Harrison, Implications of till deformation on glacier dynamics, *J. Glaciol.*, *47*, 123–134, 2001.

Walder, J. S., Hydraulics of subglacial cavities, *J. Glaciol.*, *32*, 439–445, 1986.

Willis, I. C., M. J. Sharp, and K. S. Richards, Configuration of the drainage system of Midtdalsbreen, Norway, as indicated by dye-tracing experiments, *J. Glaciol.*, *36*, 89–101, 1990.

D. Mair, Department of Geography and Environment, University of Aberdeen, Elphinstone Road, Aberdeen AB24 3UF, UK. (d.mair@abdn.ac.uk)

P. Nienow, Department of Geography and Topographic Sciences, University of Glasgow, Glasgow G12 8QQ, UK. (pnienow@geog.gla.ac.uk)

M. Sharp and T. Wohlleben, Department of Earth and Atmospheric Sciences, University of Alberta, 1-26 Earth Science Bldg., Edmonton, Alberta, Canada T6G 2E3. (martin.sharp@ualberta.ca)

I. Willis, Department of Geography, University of Cambridge, Cambridge CB2 3EN, UK.